J|A|C|S
ARTICLES
Published on Web 07/13/2006

MIL-96, a Porous Aluminum Trimesate 3D Structure Constructed from a Hexagonal Network of 18-Membered Rings and μ_3-Oxo-Centered Trinuclear Units

Thierry Loiseau,*[,†] Ludovic Lecroq,[†] Christophe Volkringer,[†] Jérôme Marrot,[†] Gérard Férey,[†,‡] Mohamed Haouas,[§] Francis Taulelle,[§] Sandrine Bourrelly,[||] Philip L. Llewellyn,[||] and Michel Latroche[⊥]

Contribution from the Institut Lavoisier (UMR CNRS 8180), Institut Universitaire de France, Porous Solids Group, Tectospin, Université de Versailles Saint Quentin en Yvelines, 45, avenue des Etats-Unis, 78035 Versailles, MADIREL, Université de Provence (UMR CNRS 6121), Centre Saint Jérôme, 13397 Marseille Cedex 20 and LCMTR (UPR CNRS 209), 2-8, rue Henri Dunant, 94320 Thiais, France

Received April 6, 2006; E-mail: loiseau@chimie.uvsq.fr

Abstract: A new aluminum trimesate $Al_{12}O(OH)_{18}(H_2O)_3(Al_2(OH)_4)[btc]_6 \cdot 24H_2O$, denominated MIL-96, was synthesized under mild hydrothermal conditions (210 °C, 24 h) in the presence of 1,3,5-benzenetricarboxylic acid (trimesic acid or *H₃btc*) in water. Hexagonal crystals, allowing a single-crystal XRD analysis, are grown from a mixture of trimethyl 1,3,5-benzenetricarboxylate (*Me₃btc*), HF, and TEOS. The MIL-96 structure exhibits a three-dimensional (3D) framework containing isolated trinuclear μ_3-oxo-bridged aluminum clusters and infinite chains of $AlO_4(OH)_2$ and $AlO_2(OH)_4$ octahedra forming a honeycomb lattice based on 18-membered rings. The two types of aluminum groups are connected to each other through the trimesate species, which induce corrugated chains of aluminum octahedra, linked via μ_2-hydroxo bonds with the specific *-cis−cis−trans-* sequence. The 3D framework of MIL-96 reveals three types of cages. Two of them, centered at the special positions 0 0 0 and $^2/_3$ $^1/_3$ $^1/_4$, have estimated pore volumes of 417 and 635 Å^3, respectively, and encapsulate free water molecules. The third one has a smaller pore volume and contains disordered aluminum octahedral species ($Al(OH)_6$). The solid-state NMR characterization is consistent with crystal structure and elemental and thermal analyses. The four aluminum crystallographic sites are resolved by means of ^{27}Al 3QMAS technique. This product is able to sorb both carbon dioxide and methane at room temperature (4.4 mmol·g^{-1} for CO_2 and 1.95 mmol·g^{-1} for CH_4 at 10 bar) and hydrogen at 77 K (1.91 wt % under 3 bar).

Introduction

In the past decade, there has been an increasing interest in the synthesis of porous metal−organic framework materials (MOF) or coordination polymers,[1−3] based on the connection of metal ions (nodes) and organic ligands (linkers), such as amines or carboxylates, usually including one or several benzene rings. These solids exhibit novel fascinating three-dimensional (3D) topologies, which may potentially find applications as molecular sieves and gas adsorbents (for instance, hydrogen or methane storage[4]), ion exchange or heterogeneous catalysis.[5,6] Some of them possess rigid open-frameworks, which are reminiscent to the functionalities observed in the microporous aluminosilicates networks (zeolites). The carboxylate family has attracted more attention since extra-large pore solids with relative high thermal stability have been synthesized. This series is well illustrated with the examples of the MOF-*n* solids (MOF-5,[7] MOF-177[8]) by Yaghi, or MIL-100[9] and MIL-101[10] compounds by Férey. Usually, 3d divalent (Ni^{2+}, Cu^{2+}, Zn^{2+}) and trivalent (Sc^{3+}, V^{3+}, Cr^{3+}, Fe^{3+}) or rare earth metals are used as metallic centers, but the trivalent p elements such as Al^{3+}, Ga^{3+} or In^{3+} are much more rarely reported. Recently, a systematic investigation of the reactivity of indium with the benzene-based carboxylates was described by different groups.[11−17] The use of aluminum or gallium for the production

† Institut Lavoisier, Porous Solids Group.
‡ Institut Universitaire de France.
§ Institut Lavoisier, Tectospin.
|| MADIREL, Université de Provence.
⊥ LCMTR, Thiais.

(1) Batten, S. R.; Robson, R. *Angew. Chem., Int. Ed. Engl.* **1998**, *37*, 1460.
(2) Moulton, B.; Zaworotko, M. J. *Chem. Rev.* **2001**, *101*, 1629.
(3) Yaghi, O. M.; O'Keeffe, M.; Ockwig, N. W.; Chae, H. K.; Eddaoudi, M.; Kim, J. *Nature* **2003**, *423*, 705.
(4) Fletcher, A. J.; Thomas, K. M.; Rosseinsky, M. J. *J. Solid State Chem.* **2005**, *178*, 2491.
(5) Janiak, C. *Dalton Trans.* **2003**, 2781.
(6) Kitagawa, S.; Kitaura, R.; Noro, S.-I. *Angew. Chem., Int. Ed.* **2004**, *43*, 2334.
(7) Li, H.; Eddaoudi, M.; O'Keeffe, M.; Yaghi, O. M. *Science* **1999**, *402*, 276.
(8) Chae, H. K.; Siberio-Pérez, D. Y.; Kim, J.; Go, Y. B.; Eddaoudi, M.; Matzger, A. J.; O'Keeffe, M.; Yaghi, O. M. *Nature* **2004**, *427*, 523.
(9) Férey, G.; Serre, C.; Mellot-Draznieks, C.; Millange, F.; Surblé, S.; Dutour, J.; Margiolaki, I. *Angew.* Chem., Int. Ed. **2004**, *43*, 6296.
(10) Férey, G.; Mellot-Draznieks, C.; Serre, C.; Millange, F.; Dutour, J.; Surblé, S.; Margiolaki, I. *Science* **2005**, *309*, 2040.
(11) Gomez-Lor, B.; Gutierrez-Puebla, E.; Monge, M. A.; Ruiz-Valero, C.; Snejko, N. *Inorg. Chem.* **2002**, *41*, 2429.

of MOFs materials is less common, despite a rich literature[18,19] relating to the chemistry of molecular aluminum carboxylate complexes for their neurotoxic effects in biological systems or alumoxanes species resulting from the reaction of carboxylic acids with boehmite.[20−22] On the other hand, the hydrolysis of aluminum in aqueous solution has been intensively studied for over 40 years.[23] Besides the isolation of large purely inorganic aggregates such as Al_{13}[24−26] or Al_{30}[26,27] polycations species, novel clusters such as the Al_{13}[28] and Al_4[29] or Al_{15}[30] species are formed in the presence of the carboxylate ligands *heidi* (*H*$_3$*heidi* = $N(CH_2COOH)_2(CH_2CH_2OH)$) and *hpdta* (*H*$_5$*hpdta* = $HOCH_2$-$[CH_2N(CH_2COOH)_2]_2$), respectively.

The group in Versailles focuses its attention on the reaction of aluminum or gallium with aromatic carboxylic acids under hydrothermal conditions. Up to now, two phases have been isolated with aluminum, MIL-53[31] (with 1,4-benzenedicarboxylic acid or *H*$_2$*bdc*) and MIL-69[32] (with 2,6-naphthalenedicarboxylic acid or *H*$_2$*ndc*), and one for gallium, MIL-61[33] (with 1,2,4,5-benzenetetracarboxylic acid or *H*$_4$*btec*). The MIL-53 compound was found to be a good candidate for H_2,[34] CH_4, and CO_2[35] adsorption, and significant uptake values were observed for these different gases, partly due to the low density of these materials with aluminum being a relatively light element. We continue these series with the utilization of the trimesic acid ligand (1,3,5-benzenetricarboxylic acid or *H*$_3$*btc*). Under some conditions, a ladder-like pure fluoride aluminum $([Al_2F_8]^{2-})_n$ species[36] intercalated by the triprotonated *H*$_3$*btc* molecules was previously obtained with the HF/pyridine solvent mixture. Here, this contribution addresses the synthesis and characterization of a new 3D framework, noted MIL-96 (Al), $Al_{12}O(OH)_{18}(H_2O)_3(Al_2(OH)_4)[btc]_6{\cdot}24H_2O$ involving the aluminum octahedral units interacting with the *btc* ligand. We applied an alternative synthesis route for growing well-defined single crystals of such MOF solids by using the methyl ester form (trimethyl 1,3,5-benzenetricarboxylate or *Me*$_3$*btc*) of the trimesic acid together with HF and TEOS. The arrangement of the metallic cation Al^{3+} in this particular solid is new and original for the chemistry of aluminum since isolated μ_3-oxo-centered trinuclear units and a two-dimensional (2D) network of hexagonal 18-membered rings are observed. The MIL-96 (Al) compound is characterized by means of single-crystal X-ray analysis, ^{27}Al solid-state MAS NMR and gas adsorption was reported for CO_2, CH_4, and H_2.

Experimental Section

Synthesis. The aluminum trimesate $Al_{12}O(OH)_{18}(H_2O)_3(Al_2(OH)_4)[btc]_6{\cdot}24H_2O$ (MIL-96) was hydrothermally synthesized under autogenous pressure from a mixture of aluminum nitrate and 1,3,5-benzenetricarboxylic acid in water. The starting reactants were aluminum nitrate ($Al(NO_3)_3{\cdot}9H_2O$, Carlo Erba Regenti, 98%), 1,3,5-benzenetricarboxylic acid ($C_6H_3(CO_2H)_3$, Aldrich, 95%, or *H*$_3$*btc*). In addition, different synthesis batches used trimethyl 1,3,5-benzenetricarboxylate ($C_6H_3(CO_2CH_3)_3$, 98%, Aldrich, noted *Me*$_3$*btc*), diluted hydrofluoric acid (HF, Normapur, 4.8%) and tetraethylortho silicate ($Si(OC_2H_5)_4$, TEOS, Merck, >98%). Typically, the reaction mixture containing the molar ratio: 1 $Al(NO_3)_3{\cdot}9H_2O$ (3.5 mmol, 1.314 g)/0.14 *H*$_3$*btc* (0.5 mmol, 0.105 g)/80 H_2O (278 mmol, 5 mL) was placed in a 23-mL Teflon-lined steel Parr autoclave at 210 °C for 24 h (batch **1**). The pH of synthesis was 1. After the hydrothermal treatment, a powdered product was obtained, which was filtered off, washed with deionized water, and dried in air at room temperature. Optical microscope analysis indicated that the sample is composed of a mixture of a fine white powder (~1 μm size) of the title compound and large parallelepiped-shaped crystals of recrystallized *H*$_3$*btc* ($C_9H_6O_6{\cdot}0.83H_2O$[37] form). Preliminary X-ray powder diffraction pattern showed that the fine powder is a novel phase. The MIL-96 (Al) phase could be obtained as a pure phase by using the trimethyl 1,3,5-benzenetricarboxylate as starting reactant (batch **2**). The reaction mixture was 1 $Al(NO_3)_3{\cdot}9H_2O$ (3.5 mmol, 1.314 g)/0.5 *Me*$_3$*btc* (1.75 mmol, 0.440 g)/80 H_2O (278 mmol, 5 mL), and a pure phase of MIL-96 (Al) is prepared after heating for 24 h at 210 °C under hydrothermal conditions. Suitable single-crystals for XRD analysis were obtained from a different mixture (batch **3**). In this case, the reaction molar composition was 1 $Al(NO_3)_3{\cdot}9H_2O$ (3.5 mmol, 1.314 g)/0.5 *Me*$_3$*btc* (1.75 mmol, 0.440 g)/0.4 HF (1.4 mmol, 0.6 mL)/0.2 TEOS (0.7 mmol, 0.16 mL)/320 H_2O (1111 mmol, 20 mL). HF[38] and TEOS[39] are used for their mineralizing effect under hydrothermal conditions, inducing the increased crystallinity. These reactants were placed in a 125-mL Teflon-lined steel Parr autoclave at 210 °C for 24 h, and flat hexagonal-shape crystals of 10−40 μm size were obtained in the absence of recrystallized *H*$_3$*btc*.

Single-Crystal X-ray Structure Analysis. A colorless hexagonal-shaped crystal (0.04 mm × 0.04 mm × 0.04 mm) was selected under polarizing optical microscope and glued on a glass fiber for a single-crystal X-ray diffraction experiment. X-ray intensity data were collected on a Bruker ×8-APEX2 CCD area-detector diffractometer using Mo Kα radiation (λ = 0.71073 Å). Four sets of narrow data frames (60 s per frame) were collected at different values of θ for 2 and 2 initial values of ϕ and ω, respectively, using 0.3° increments of ϕ or ω. Data reduction was accomplished using SAINT V7.03. The substantial redundancy in data allowed a semiempirical absorption correction (SADABS V2.10) to be applied, on the basis of multiple measurements of equivalent reflections. The structure was solved in the space group $P6_3/mmc$ by direct methods, developed by successive difference Fourier

(12) Lin, Z.-Z.; Luo, J.-H.; Hong, M.-C.; Wang, R.-H.; Han, L.; Cao, R. *J. Solid State Chem.* **2004**, *177*, 2494.
(13) Gomez-Lor, B.; Gutierrez-Puebla, E.; Iglesias, M.; Monge, M. A.; Ruiz-Valero, C.; Snejko, N. *Chem.* Mater. **2005**, *17*, 2568.
(14) Lin, Z.; Jiang, F.; Chen, L.; Yuan, D.; Hong, M. *Inorg. Chem.* **2005**, *44*, 73.
(15) Lin, Z.-Z.; Jiang, F.-L.; Chen, L.; Yuan, D.-Q.; Zhou, Y.-F.; Hong, M.-C. *Eur. J. Inorg. Chem.* **2005**, 77.
(16) Lin, Z.-Z.; Jiang, F.-L.; Yuan, D.-Q.; Chen, L.; Zhou, Y.-F.; Hong, M.-C. *Eur. J. Inorg. Chem.* **2005**, 1927.
(17) Lin, Z.; Chen, L.; Jiang, F.; Hong, M. *Inorg. Chem. Commun.* **2005**, *8*, 199.
(18) Powell, A. K.; Heath, S. L. *Coord. Chem. Rev.* **1996**, *149*, 59.
(19) Salifoglou, A. *Coord. Chem. Rev.* **2002**, *228*, 297.
(20) Landry, C. C.; Pappé, N.; Mason, M. R.; Apblett, A. W.; Tyler, A. N.; MacInnes, A. N.; Barron, A. R. *J.* Mater. Chem. **1995**, *5*, 331.
(21) Bethley, C. E.; Aitken, C. L.; Harlan, C. J.; Koide, Y.; Bott, S. G.; Barron, A. R. *Organometallics* **1997**, *16*, 329.
(22) Narayanan, R.; Laine, R. M. *J. Mater. Chem.* **2000**, *10*, 2097.
(23) Casey, W. H. *Chem. Rev.* **2006**, *106*, 1.
(24) Johansson, G. *Arkiv. Kem.* **1962**, *20*, 305.
(25) Seichter, W.; Mögel, H.-J.; Brand, P.; Salah, D. *Eur. J. Inorg. Chem.* **1998**, 795.
(26) Rowsell, J.; Nazar, L. F. *J. Am. Chem. Soc.* **2000**, *122*, 3777.
(27) Allouche, L.; Gérardin, C.; Loiseau, T.; Férey, G.; Taulelle, F. *Ang. Chem., Int. Ed.* **2000**, *39*, 511.
(28) Heath, S. L.; Jordan, P. A.; Johnson, I. D.; Moore, G. R.; Powell, A. K.; Helliwell, M. *J. Inorg. Biochem.* **1995**, *59*, 785.
(29) Schmitt, W.; Jordan, P. A.; Henderson, R. K.; Moore, G. R.; Anson, C. E.; Powell, A. K. *Coord. Chem.* Rev. **2002**, *228*, 115.
(30) Schmitt, W.; Baissa, E.; Mandel, A.; Anson, C. E.; Powell, A. K. *Ang. Chem., Int. Ed.* **2001**, *40*, 3578.
(31) Loiseau, T.; Serre, C.; Huguenard, C.; Fink, G.; Taulelle, F.; Henry, M.; Bataille, T.; Férey, G. *Chem.* Eur. J. **2004**, *10*, 1373.
(32) Loiseau, T.; Mellot-Draznieks, C.; Muguerra, H.; Férey, G.; Haouas, M.; Taulelle, F. *C. R. Chimie* **2005**, *8*, 765.
(33) Loiseau, T.; Muguerra, H.; Haouas, M.; Taulelle, F.; Férey, G. *Solid State Sci.* **2005**, *7*, 603.
(34) Férey, G.; Latroche, M.; Serre, C.; Millange, F.; Loiseau, T.; Percheron-Guégan, A. *Chem. Commun.* **2003**, 2976.
(35) Bourrelly, S.; Llewellyn, P. L.; Serre, C.; Millange, F.; Loiseau, T.; Férey, G. *J. Am. Chem. Soc.* **2005**, *127*, 13519.
(36) Loiseau, T.; Muguerra, H.; Marrot, J.; Férey, G.; Haouas, M.; Taulelle, F. *Inorg. Chem.* **2005**, *44*, 2920.
(37) Herbstein, F. H.; Marsh, R. E. *Acta Crystallogr. B* **1977**, *33*, 2358.
(38) Caullet, P.; Paillaud, J.-L.; Simon-Masseron, A.; Soulard, M.; Patarin, J. *C. R. Chimie* **2005**, *8*, 245.
(39) Kan, Q.; Glasser, F. P.; Xu, R. *J. Mater. Chem.* **1993**, *3*, 983.

Table 1. Crystal Data and Structure Refinement for $Al_{12}O(OH)_{18}(H_2O)_3(Al_2(OH)_4)[btc]_6 \cdot 24H_2O$ (MIL-96)

identification code	MIL96 (Al)
empirical formula	$C_6H_2Al_{1.56}O_{7.33}$
formula weight	233.38
temperature	293(2) K
wavelength	0.71073 Å
crystal system, space group	hexagonal, $P6_3/mmc$
unit cell dimensions	$a = 14.2074(2)$ Å
	$b = 14.2074(2)$ Å
	$c = 31.2302(9)$ Å, $\gamma = 120°$
volume	5459.27(19) Å^3
Z, calculated density	18, 1.278 Mg/m^3
absorption coefficient	0.219 mm^{-1}
$F(000)$	2104
crystal size	0.04 × 0.04 × 0.04 mm
θ range for data collection	1.30−24.99°
limiting indices	$-16 \le h \le 16$
	$-16 \le k \le 16$
	$-37 \le l \le 34$
reflections collected/unique	65893/1858
	[R(int) = 0.0910]
completeness to $\theta = 24.99$	100.0%
refinement method	full-matrix least-squares on F^2
data/parameters	1858/125
goodness-of-fit on F^2	1.139
final R indices [$I > 2\sigma(I)$]	R1 = 0.0509, wR2 = 0.1578
R indices (all data)	R1 = 0.0717, wR2 = 0.1807
largest diff. peak and hole	0.930 and −0.856 e·Å^{-3}

syntheses, and refined by full-matrix least-squares on all F^2 data using SHELXTL V6.12. Hydrogen atoms were included in calculated positions and allowed to ride on their parent atoms. Three unique aluminum atoms (Al1, Al2, and Al3) were first revealed, and the remaining atoms (O, C, N) were placed from successive Fourier map analyses. At this stage, electron density residues (∼8 e$^-$·Å^3) were observed nearby the terminal atoms O5 (bonded to Al2) at ∼1.80 Å, suggesting the presence of an additional aluminum atom on the 12k site (Al4). However, due to its steric hindrance a partial occupancy was assumed for this aluminum and it was fixed to 1/3 in agreement with the balance of the electronic charges of the structure. Electron residues assigned to the oxygen atoms O11, O12, and O13 (with occupancy fixed to $^1/_3$) are found in the surrounding of Al4 with unrealistically short Al−O distances, and this would reflect average position due to the aluminum disorder. The hydrogen atoms were placed using geometrical constraints for the trimesate species. The population ratio between these four aluminum sites Al1:Al2:Al3:Al4 was as follows: 3:6:3:2, respectively. The final refinement including anisotropic thermal parameters of all non-hydrogen atoms converged to R1 = 0.0509 and wR2 = 0.1578 All the calculations were performed using the SHELX-TL program on the basis of F^2. The crystal data are given in Table 1. The chemical formula deduced from the X-ray diffraction analysis is the following: $Al_{12}O(OH)_{18}(H_2O)_3(Al_2(OH)_4)[btc]_6 \cdot 2H_2O$.

Thermogravimetric Analysis. The thermogravimetric analysis (under O_2, 2 °C·min^{-1}, TA Instrument 2050) of the pure phase of MIL-96 (batch **2**) shows a two-step weight loss. The first event is assigned to the continuous removal of water (free molecules trapped within the cavities and water bonded to aluminum atoms). It corresponds to 19% at 200 °C and ∼24 free water molecules per Al_{12} unit. The second weight loss is attributed to the decomposition of the structure with the departure of the trimesate species at 300 up to 580 °C (obs: 50.5%; calc: 50.8%). The final residue is Al_2O_3 with a remaining weight of 30.5% of the original value (calc: 28.9%). The deduced chemical formula for MIL-96 (Al) is $Al_{12}O(OH)_{18}(H_2O)_3(Al_2(OH)_4)[btc]_6 \cdot 24H_2O$. The X-ray thermodiffraction experiment (in air) indicated that the MIL-96 structure is stable upon water removal and collapsed at 320 °C. The chemical analyses gave 25.5% (calc: 26.0%) for C and 3.1% (calc: 3.7%) for H and are in good agreement with the chemical formula of MIL-96.

Solid-State NMR. All spectra were collected with a Bruker Avance 500 spectrometer using a 2.5-mm triple resonance MAS probe at room temperature. Powder samples were packed into 2.5-mm ZrO_2 rotors. ^{27}Al (130.3 MHz) spectra were referenced to external alum ($(NH)_4Al(SO_4)_2 \cdot 12H_2O$) at −0.6 ppm relative to 1 M aqueous $Al(NO_3)_3$ as secondary reference. The radio frequency field strength was determined from nutation experiments on both cubic solid alum (liquidlike behavior) and solid nutation of berlinite $AlPO_4$. The single-pulse ^{27}Al spectrum was collected at a spinning rate of 30 kHz. The experiment was recorded after excitation with $\pi/12$ pulses of 86 kHz rf power and repetition time of ∼100 ms. The 3QMAS 2D NMR experiment[40,41] was achieved at a spinning rate of 25 kHz using a z-filter sequence[42] with two hard pulses of 4.1 μs (127°) and 1.6 μs (50°) and one selective pulse of 12.2 μs (90°). Additional 3QMAS experiment with rf pulses of higher power (∼170 kHz) and fast amplitude modulation (FAM-II) method for conversion of observable coherence was run to optimize MQMAS efficiency for sites with larger quadrupolar interactions.[43] Simulations of spectra were done with the Bruker dmFit software package.

Adsorption Microcalorimetry. The apparatus used for microcalorimetry experiments is able to measure both isotherms and experimental enthalpies of adsorption in the temperature region from 25 to 150 °C.[44] The Tian-Calvet type microcalorimeter used to measure the enthalpies consists of two thermopiles mounted in electrical opposition. Each thermopile comprises ∼500 chromel−alumel thermocouples. The adsorption isotherms are obtained using a manometric device built to withstand pressures up to 100 bar. The pressure gauge measures pressures up to 50 bar. A point-by-point introduction of gas is most adapted to this system. Each introduction of adsorbate to the sample is accompanied by an exothermic thermal effect, until equilibrium is attained. This peak in the curve of energy with time has to be integrated to provide an integral (or pseudodifferential) molar enthalpy of adsorption for each dose. The calorimetric cell (including the relevant amounts of adsorbent and gas) is considered as an open system. In this procedure, it is important to consider that the gas is introduced reversibly. Under these conditions it is possible to determine the differential enthalpy of adsorption $\Delta_{ads}h$, via the following expression:

$$\Delta_{ads}h = \left(\frac{dQ_{rev}}{dn^a}\right)_T + V_c\left(\frac{dp}{dn^a}\right)_T$$

Here dQ_{rev} is the heat reversibly exchanged with the surrounding environment at temperature T, as measured by the calorimeter, dn^a is the amount adsorbed after introduction of the gas dose, dp is the increase in pressure and V_c is the dead space volume of the sample cell within the calorimeter itself (thermopile). The term $V_c dp$ can be obtained via blank experiments. Prior to each adsorption experiment, the samples were outgassed using sample controlled thermal analysis, SCTA.[45,46] Around 0.3 g of each sample was thus heated under a constant residual vacuum pressure of 0.02 mbar up to a final temperature of 100 °C which was maintained until the residual pressure was less than 5 × 10^{-3} mbar. The carbon dioxide and methane were obtained form Air Liquide (Alphagaz, France) and are of 99.998% purity. These greenhouse gases have been chosen with respect to their interest in several applications. From a more fundamental point of view, a comparison between a probe molecule with a significant quadrupole moment and one without any permanent moment can be beneficial for the characterization of adsorbents.

(40) Frydman, L.; Harwood: J. S. *J. Am. Chem. Soc.* **1995**, *117*, 5367.
(41) Medek, A.; Harwood: J. S.; Frydman, L. *J. Am. Chem. Soc.* **1995**, *117*, 12779.
(42) Fernandez, C.; Delevoye, L.; Amoureux, J.-P.; Lang, D. P.; Pruski, M. *J. Am. Chem. Soc.* **1997**, *119*, 6858.
(43) Morais, C. M.; Lopes, M.; Fernandez, C.; Rocha, J. *Magn. Reson. Chem.* **2003**, *41*, 679.
(44) Llewellyn, P. L.; Maurin, G. *C. R. Chimie* **2005**, *8*, 283.
(45) Rouquerol, J. *Thermochim. Acta* **1989**, *144*, 209.
(46) Sorensen, O. T.; Rouquerol, J. *in "Sample Controlled Thermal Analysis", Kluwer Acad. Dordrecht.* **2003**.

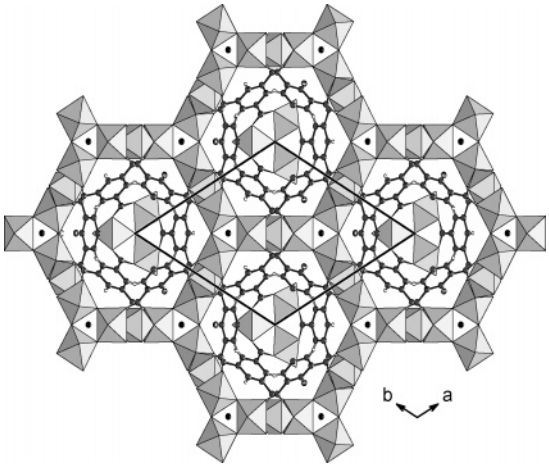

Figure 1. Projection of the structure of MIL-96 (Al) along the *c* axis, showing the hexagonal network of the aluminum octahedra (gray) containing 18-membered rings connected to the μ_3-oxo-centered trinuclear units, via the trimesate ligand. Water molecules: black.

Hydrogen Storage Measurements. Hydrogen storage measurements were made using a volumetric device (Sievert's method) equipped with calibrated and thermalized volumes and pressure gauges. About 1 g of powder was transferred into a tight stainless steel sample holder. The sample was then outgassed at 150 °C during 18 h under primary vacuum. At the end of the experiment, the sample holder was transferred into a glovebox under purified argon and weighed again to measure the mass loss from the dehydrated sample. All weight capacities refer here to outgassed samples. For adsorption measurements at 77 K, the sample holder was immersed in liquid nitrogen and high-purity hydrogen (Alphagaz H22) was introduced step by step in the container up to 0.41 MPa. The pressure variations due to both gas cooling and hydrogen adsorption were measured as a function of time. Under these thermodynamic conditions ($0 < P < 1$ MPa; $T = 77$ K), the ideal gas law is no longer valid, and a different equation of state was used for this pressure and temperature range.[47]

Results and Discussion

Structure Description. The MIL-96 (Al) phase exhibits a 3D framework (Figure 1) consisting of the connection of octahedrally coordinated aluminum, which are linked through the trimesate ligand, $[btc]^{3-}$. The presence of the $[btc]^{3-}$ ligand in the structure indicates that the trimethyl 1,3,5-benzenetricarboxylate ester is hydrolyzed into the carboxylate form, which further reacted with the aluminum cations under hydrothermal conditions. Here, the use of the methyl ester form of the carboxylic acid has a drastical effect on the synthesis conditions since no recrystallization of the trimesic acid is observed and a pure form of the MIL-96 (Al) is obtained. The method of the in situ carboxylate ligand synthesis was previously reported for the formation of 3D coordination polymers, and it was reported that the hydrothermal in situ slow hydrolysis reaction improved the crystallization process for the crystal engineering of such compounds.[48,49] Using this strategy, analogous compounds of MIL-96 have been prepared with gallium[50] and indium[51] and will be discussed elsewhere.

Two distinct inorganic blocks have been found in the MIL-96 framework. The first one (Figure 2) is a discrete trinuclear

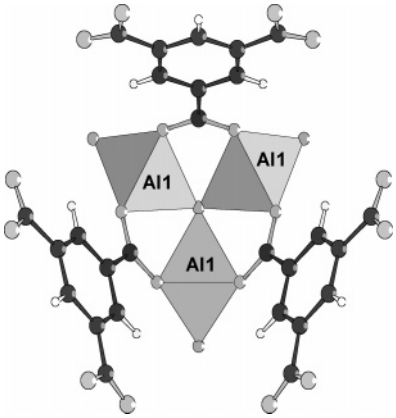

Figure 2. View of the μ_3-oxo-centered trinuclear $Al_3(\mu_3\text{-}O)[(O_2C\text{-}C_6H_3\text{-}(CO_2)_2]_6(H_2O)_3$ core in MIL-96, showing the three $AlO_5(H_2O)$ octahedral units (site Al1) chelated by the trimesate groups (black circles: carbon; open circles: hydrogen; gray circles: oxygen).

moiety with the aluminum octahedra $AlO_5(H_2O)$, corner-sharing a μ_3-oxo centered group (corresponding to the crystallographic site Al1 (6h)). The four equatorial Al−O distances are 1.889(2) Å while the Al−μ_3-O is shorter (1.834(2) Å). The remaining oxygen atom belongs to a coordinated water molecule, which is *trans* to the Al−μ_3-O bond. It corresponds to a longer Al−O distance (1.945(5) Å), and this is in good agreement with valence bond calculations[52] (expected value for H_2O: 0.4, calculated: 0.45). This type of trimeric oxo-centered carboxylate-bridged cluster formulated as $[M_3O(O_2CR)_6L_3]^+$ (L = H_2O, N, ...) is quite well-known for many trivalent transition metals such as V, Cr, Mn, Fe, Co, Ru, Rh, Ir, and Pt.[53] Most of these phases have been isolated using the acetate species, but more recently, such triangular metal-centered units have been encountered in phases crystallizing with aromatic polycarboxylates.[9,10,54−57] However, to our knowledge, this is the first time that such a trinuclear configuration is observed in aluminum chemistry. Indeed, only one trimeric complex was reported with aluminum. It is a cluster stabilized by citric acid[58,59] exhibiting a different configuration; it consists of two aluminum octahedra sharing an edge (μ_2-OH) connected to a third aluminum octahedron by corner μ_2-O bridges. On the other hand, trimer of aluminum can be extracted from the structural description of the brucite-like polycation flat-Al_{13}[25] or the Keggin-type species ϵ-Al_{13}[24] and δ-Al_{13}[26] for which each face of the motif is composed of three aluminum octahedral sharing edges.

The second inorganic part consists of a 2D network containing chains of aluminum $AlO_2(OH)_4$ and $AlO_4(OH)_2$ octahedra, interconnected with each other to generate a hexagonal 18-membered ring in the (*a*,*b*) plane (Figure 1). There are two crystallographically inequivalent types of aluminum, Al2 and Al3, which are respectively coordinated to four and two oxygen atoms coming from the carboxylate groups of the trimesate molecule and four and two bridging μ_2-hydroxo moieties: the

(47) Younglove, B. A. *J. Phys. Chem. Ref. Data* **1982**, *11*, 1.
(48) Evans, O. R.; Lin, W. *Acc. Chem. Res.* **2002**, *35*, 511.
(49) Zhang, X.-M. *Coord. Chem. Rev.* **2005**, *249*, 1201.
(50) Volkringer, C.; Loiseau, T.; Férey, G.; Morais, C.; Taulelle, F.; Montouillout, V.; Massiot, D. **2006**, in preparation.
(51) Volkringer, C.; Loiseau, T. *Mater. Res. Bull.* **2006**, *41*, 948.
(52) Brese, N. E.; O'Keeffe, M. *Acta Crystallogr. B* **1991**, *47*, 192.
(53) Cotton, F. A.; Wilkinson, G. *in "Advanced Inorganic Chemistry", Fifth Edition, John Wiley & Sons:* **1988**.
(54) Barthelet, K.; Riou, D.; Ferey, G. *Chem. Commun.* **2002**, 1492.
(55) Serre, C.; Millange, F.; Surblé, S.; Férey, G. *Ang. Chem., Int. Ed.* **2004**, *43*, 6285.
(56) Sudik, A. C.; Côté, A. P.; Yaghi, O. M. *Inorg. Chem.* **2005**, *44*, 2998.
(57) Férey, G.; Mellot-Draznieks, C.; Serre, C.; Millange, F. *Acc. Chem. Res.* **2005**, *38*, 217.
(58) Feng, T. L.; Gurian, P. L.; Healy, M. D.; Barron, A. R. *Inorg. Chem.* **1990**, *29*, 408.
(59) Malone, S. A.; Cooper, P.; Heath, S. L. *Dalton Trans.* **2003**, 4572.

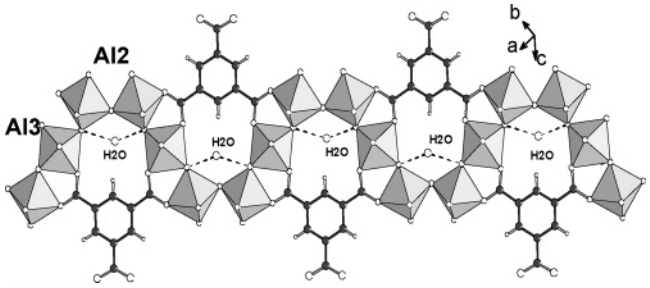

Figure 3. View of the corrugated chains of corner-sharing aluminum octahedral, with the *-cis−cis−trans* sequence corresponding to the −Al2−OH−Al2−OH−Al3- bonding scheme, in MIL-96. The hydrogen-bond interaction scheme is shown between the water molecule and the μ_2-OH groups bridging the aluminum atoms Al2 and Al3.

two oxo groups are in *cis* positions for Al2, whereas the hydroxo groups are in *trans* positions for Al3, with typical Al−O distances. The lengths of the Al2−OH bonds are in the range 1.837(1)−1.893(1) Å, and the Al2−O bond is longer at 1.906-(2) Å (Al2−O8)). The Al3−O6 distances correspond to the value of 1.862(1) Å, whereas the length of the Al3−OH bond is shorter at 1.836(1) Å (Al3−O2). The hydroxo groups are in a bridging position between two aluminum atoms. The valence bond calculations[52] give values in the range 1.189−1.210 for oxygen atoms bridging aluminum, which are close to the expected value (1.2) for hydroxo species. This μ_2-OH connection generates original corrugated infinite chains of aluminum octahedra, with a *-cis−cis−trans-* corner-sharing sequence (Figure 3). The sinusoidal shape of the octahedra file is induced by the ternary geometry of the trimesate molecule. Such a configuration was already reported in other metal carboxylates synthesized with the same tribenzoic acid. For instance in a cobalt-based solid,[60] infinite chains of edge- and corner-sharing octahedra occur. In MIL-96, the particular corner-sharing octahedra connection mode differs from those previously observed in the tancoite-like solids[61,62] (straight chains with *trans* corner-sharing linkage [see for instance the MIL-53[31]/MIL-69[32] topologies]) or KTP-like materials[63,64] (zigzag chains with *-cis−trans-* corner-sharing linkage). However, an identical arrangement of such corrugated corner-sharing chains was recently encountered in the titanium phosphate, $Ti_3P_6O_{27}{\cdot}5(C_2H_{10}N_2){\cdot}2H_3O$,[65] containing a 1D chiral chain. A further aspect is the corner-sharing octahedra connection observed in MIL-96, which is in contrast with the edge-sharing mode occurring in the molecular species,[19] large polycationic forms such as Al_8,[66] Al_{13},[24,25] Al_{15},[30] or Al_{30}[26,27] or dense infinite networks such as boehmite or gibbsite.[67] This situation is also reported in the aluminum borate PKU-1,[68] which exhibits a porous framework with 18-membered ring channels. In this compound, all the AlO_6 octahedra are connected to each other through a common edge,

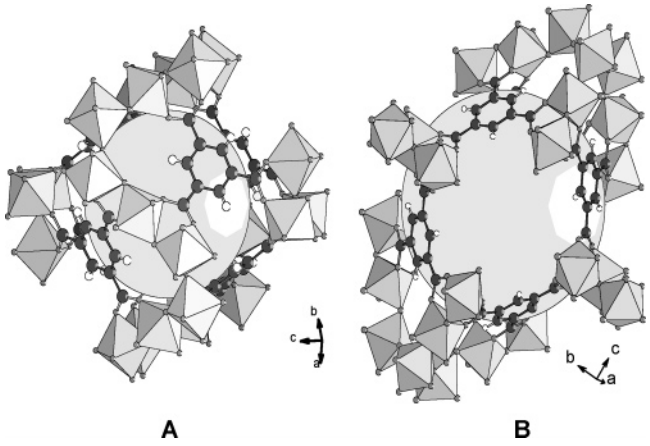

Figure 4. View of the cavities A and B in MIL-96. The light gray spheres (centered on position 0 0 0 for A and $^2/_3$ $^1/_3$ $^1/_4$ for B) indicates the empty space of the cage.

and the structure can be described from the hexagonal network of 18 aluminum centers.

The cohesion of the structure is ensured by the connection of the oxo-centered trinuclear aluminum units with the 2D network of aluminum octahedra through the trimesate molecules. This results in a 3D framework with the compact packing of three types of cavities. The first one (noted A, Figure 4) is delimited by two trinuclear units along the *c* axis connected to the 18-membered ring in the (*a*,*b*) plane via six *btc* ligands and is centered on the special position 0 0 0 (2a). The corresponding cavity-free diameter is estimated to be 8.8 Å (based on the ionic radius of 1.35 Å for oxygen) with a pore volume of ∼420 Å^3 (calculations using the PLATON[69] software, option CALC SOLV). A water molecule was clearly located within the period of one aluminum sinusoidal chain, bordered by one trimesate motif. This molecule is hydrogen-bonded to two bridging μ_2-OH groups with short $H_2O{\cdots}OH$ distances (2.917(1) Å). A second cage (noted B, Figure 4) is located at the special position $^2/_3$ $^1/_3$ $^1/_4$ (2d). It is delimited by the three trimeric μ_3-oxo-bridged aluminum units in the (*a*,*b*) plane connected to two triangular units composed of aluminum octahedra Al2 and Al3 via six *btc* species. It results in an elongated cavity along the *c* axis with a larger pore volume (∼635 Å^3).[69] For both cages A and B, the XRD analysis does not indicate any significant electronic residue, which might be assigned to trapped species such as water for instance, as observed by TG analysis. Thus, this empty space could be occupied by water molecules with a static or motional disorder, which is hardly observable by the XRD technique. The pore-opening diameters of these large cavities are rather small and were estimated in the range 2.5−3.5 Å (based on the ionic radius of 1.35 Å for oxygen). The third cavity (noted C, Figure 5) is centered around the position $^1/_3$ $^2/_3$ $^1/_4$ (2c) and situated between three trinuclear units in the (*a*,*b*) plane and two trimeric motifs containing three $AlO_2(OH)_4$ octahedra along the *c* axis. Each of these trimers corresponds to one of the hexagonal nodes of the 18-membered ring of aluminum octahedra. In fact, the Fourier map examination showed the positions of several residual peaks, with distances of 1.789 Å, suggesting the presence of an additional aluminum atom, noted Al4. This latter is surrounded by three residues (noted O11, O12, and O13) with very short unrealistic distances

(60) Livage, C.; Guillou, N.; Marrot, J.; Férey, G. *Chem. Mater.* **2001**, *13*, 4387.
(61) Hawthorne, F. C. *Tschermaks Mineral. Petrogr. Mitt.* **1983**, *31*, 121.
(62) Attfield, M. P.; Morris, R. E.; Burshtein, I.; Campana, C. F.; Cheetham, A. K. *J. Solid State Chem.* **1995**, *118*, 412.
(63) Tordjman, I.; Masse, R.; Guitel, J. C. *Z. Kristallogr.* **1974**, *139*, 103.
(64) Kirkby, S. J.; Lough, A. J.; Ozin, G. A. *Z. Kristallogr.* **1995**, *210*, 956.
(65) Guo, Y.; Shi, Z.; Yu, J.; Wang, J.; Liu, Y.; Bai, N.; Pang, W. *Chem. Mater.* **2001**, *13*, 203.
(66) Casey, W. H.; Olmstead, M. M.; Phillips, B. L. *Inorg. Chem.* **2005**, *44*, 4888.
(67) Euzen, P.; Raybaud, P.; Krokidis, X.; Toulhoat, H.; Le Loarer, J.-L.; Jolivet, J.-P.; Froidefond, C. *in* "Handbook of Porous Solids", Schüth, F., Sing, K., Weitkamp, J. Eds.; Wiley-VCH Verlag GmbH: Weinheim **2002**, 1591.
(68) Ju, J.; Lin, J.; Li, G.; Yang, T.; Li, H.; Liao, F.; Loong, C.-K.; You, L. *Ang. Chem., Int. Ed.* **2003**, *42*, 5607.
(69) Spek, A. L. *J. Appl. Crystallogr.* **2003**, *36*, 7.

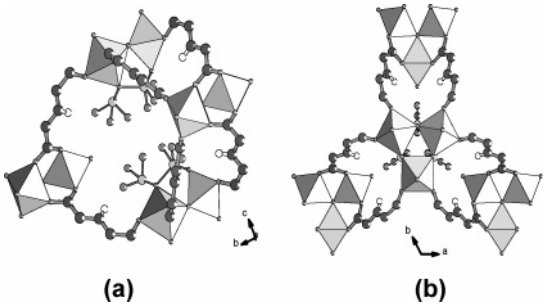

Figure 5. View of the cavity C with the additional aluminum species (Al4, pale gray) disordered on the different sites and surrounded by the different oxygen atoms (O11, O12, and O13, dark gray). (a) view along the (b,c) planes; (b) view along the *c* axis.

(1.246−1.425 Å) for Al−O, but it could be assigned to a disordering situation, for which Al is assumed to occupy the Al4 site with a factor of $^1/_3$. Indeed, within the cavity, the distances between the residues are quite short (2.7 Å), and two aluminum atoms on the Al4 site could not be face to face with each other because of the electrostatic repulsion. This involves the shift of the aluminum Al4 on one site over the three possible ones of the special position 12k. In accordance with the electroneutrality of the structure, the aluminum species Al4 would be surrounded by six hydroxo ligands. With the presence of the additional aluminum atom Al4, no empty space occurs in this third cavity.

NMR Investigations. The ^{27}Al MAS NMR spectrum of $Al_{12}O(OH)_{18}(H_2O)_3(Al_2(OH)_4)[btc]_6{\cdot}24H_2O$ (MIL-96) exhibited overlapped signals in the chemical shift range (from 20 to −40 ppm) for which aluminum is in an octahedral environment.[70] This is in perfect agreement with the XRD structure determination, which indicated that all aluminum atoms were exclusively located on hexacoordinated sites. To gain more spectral resolution, MQMAS spectroscopy has been applied. This technique combines MAS and multiquantum spectroscopy that can remove completely the second-order quadrupolar interaction.[71] Two experiments with different conditions and methods were performed. The first using the classical *z*-filter three-pulse sequence with moderate rf power (∼85 kHz) yielded three well-resolved signals with pure-absorption line shapes, shown in Figure 6. The 2D map is analyzed by modeling the quadrupolar line shape of the observed experimental signals. The second experiment used fast amplitude modulation (FAM) pulse sequence under strong rf power (∼170 kHz) conditions. Significantly better sensitivity was afforded by the FAM technique enabling evidence of a fourth site with much larger quadrupolar coupling constant (see Supporting Information). The efficiency of multiple-quantum excitation and conversion is strongly dependent on the quadrupolar frequency (ν_Q), resulting in spectra with intensities that may not quantitatively represent the relative site population. However, the resulting anisotropic line shapes that were severely distorted may be a result of the use of strong multiple-pulse rf irradiation. In this case, the lack of a full powder pattern prevented obtaining the quadrupolar parameters accurately via numerical fitting of the anisotropic line shape. It was thus possible to extract meaningful quadrupole parameters by the two combined MQMAS methods, which were used as a starting point for the simulation of the 1D MAS NMR

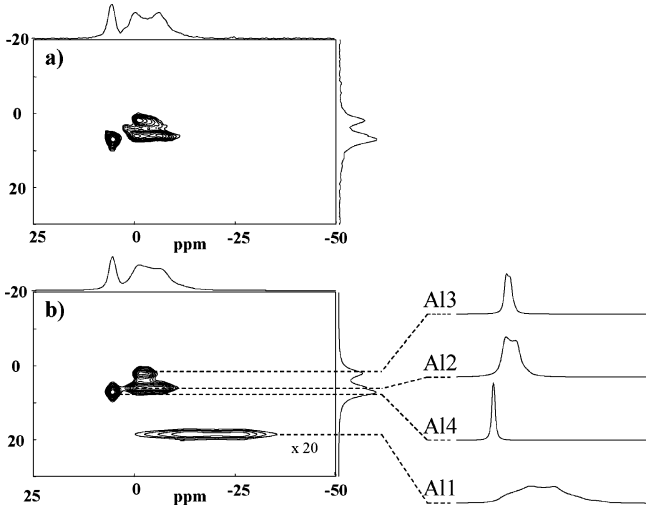

Figure 6. Experimental (a) and simulated (b) 2D ^{27}Al 3QMAS NMR spectrum of $Al_{12}O(OH)_{18}(H_2O)_3(Al_2(OH)_4)[btc]_6{\cdot}24H_2O$ (MIL-96). Four components are simulated in (b) MQMAS and slices. In (b) Al1 site, very broad, is drawn in gray with amplified intensity for sake of visualization. Its low intensity is due to the lack of efficiency of the excitation/reconversion of the triple-quantum coherences for this large QCC. Its quadrupolar parameters were estimated from an additional MQMAS experiment optimized for higher QCC, degrading consequently the low QCC sites (see Supporting Information) and from the MAS simulation (see Figure 7).

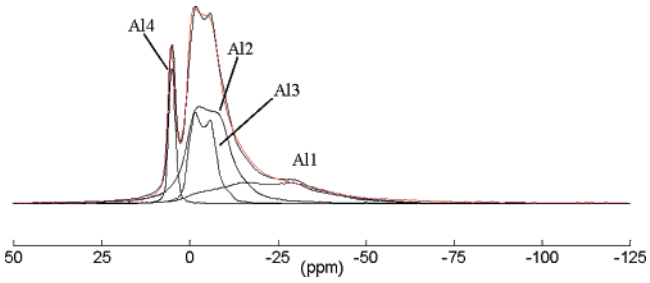

Figure 7. Experimental (red) and simulated (black) single-pulse ^{27}Al NMR spectra of $Al_{12}O(OH)_{18}(H_2O)_3(Al_2(OH)_4)[btc]_6{\cdot}24H_2O$ (MIL-96). The four components used in the decomposition are shown.

spectrum to obtain site occupancy (Figure 7). Therefore, ^{27}Al NMR resolved four distinct lines, which account for the four crystallographic sites Al1, Al2, Al3, and Al4.

The single-pulse 1D spectrum obtained with 30 kHz MAS (Figure 7) can be very well simulated with virtually identical δ_{CS}, e^2qQ/h, and η values used to simulate the MQMAS spectra. Because the resolution is better, the MQMAS results provide the most meaningful values for the second-order quadrupolar powder parameters. Table 2 summarizes data of quadrupolar patterns fits from 3QMAS experiments as well as results of MAS spectrum fits. Because of the highly contrasted NMR parameters, the structural NMR assignment of the aluminum sites can easily be done. It is based on a prior knowledge of the structural description. The signal, which has the smallest quadrupole-coupling constant, is assigned to Al4 site. Indeed, this aluminum is only partially attached to the framework, and due to its flexibility within the structure, the corresponding quadrupolar interaction would be consequently reduced. The signal with the largest quadrupole-coupling constant, which indicates the highest distortion of the Al complexes, is assigned to Al1 site of the trimeric cluster. These aluminum atoms have fewer regular Al−O distance distributions than the other Al sites due to the presence of Al−μ_3-O bonds. Moreover, the coordination of water molecules to these trimeric cluster aluminums

(70) Alemany, L. B.; Kirker, G. W. *J. Am. Chem. Soc.* **1986**, *108*, 6158.
(71) Frydman, L.; Harwood: J. S. *J. Am. Chem. Soc.* **1995**, *117*, 8367.

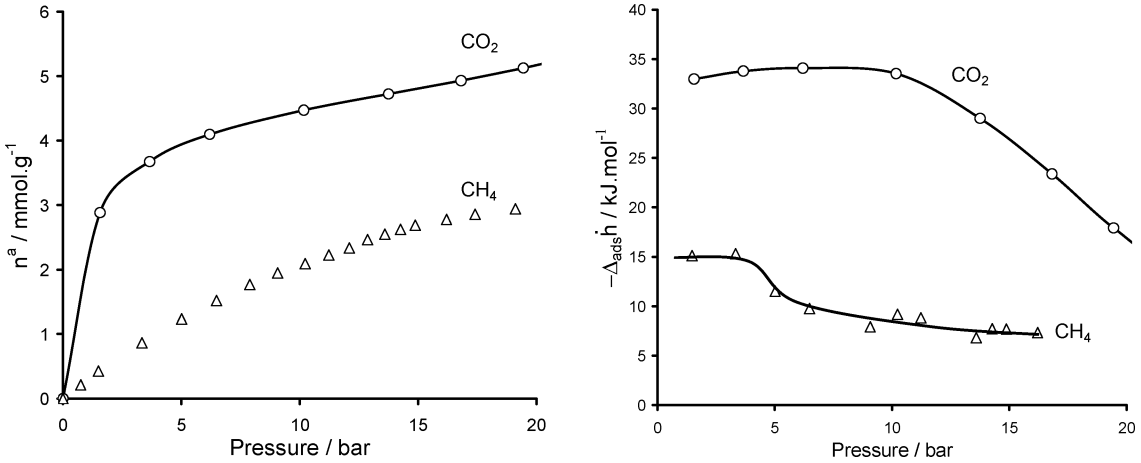

Figure 8. Isotherms (left) and differential enthalpies (right) obtained for the adsorption of carbon dioxide and methane on MIL-96 (Al) at 30 °C.

Table 2. Data of Al Sites Present in $Al_{12}O(OH)_{18}(H_2O)_3(Al_2(OH)_4)[btc]_6 \cdot 24H_2O$ (MIL-96) from Simulation of the ^{27}Al MAS NMR Spectra Obtained in Both 3QMAS (Figure 6) and Single Pulse Experiments (Figure 7)

NMR experiment	site	intensity[a]	QCC[b]	η[c]	δ_{iso}[d]
3QMAS	Al1	−	7.9	0.49	3.7
	Al2	−	4.2	0.03	2.2
	Al3	−	2.8	0.30	0.3
	Al4	−	1.7	0.56	6.5
single pulse	Al1	23%	8.2	0.49	3.1
	Al2	45%	4.7	0.03	2.4
	Al3	22%	4.0	0.30	1.8
	Al4	10%	1.9	0.56	6.4

[a] Accuracy: ±4%. [b] Quadrupole coupling constant QCC = $(e^2qQ)/h$, with the *z*-component, $V_{zz} = eq$, of the electric field gradient, the electric quadrupole moment, eQ, of ^{27}Al nuclei, and Planck's constant, h. Accuracy: ±0.6 MHz. [c] Asymmetry parameter $\eta = (V_{xx} - V_{yy})/V_{zz}$ as a function of the *x*-, *y*-, and *z*-components of the electric field gradient. Accuracy: ±0.03. [d] Isotropic chemical shift. Accuracy: ±0.8 ppm.

contributes to more disorder within their local environments. The most intense signal is attributed to the Al2 site since this aluminum is the most abundant crystallographic site. Finally, the Al3 site would present a relatively moderate quadrupole coupling constant as it is sitting on a special crystallographic position. According to these signal attributions, line integrals agree with the crystallographic stoichiometry of $Al_{12}O(OH)_{18}(H_2O)_3(Al_2(OH)_4)[btc]_6 \cdot 24H_2O$. In the chemical formula of MIL-96, 14 aluminums are associated to four different sites: Al1:A2:Al3:Al4, respecting the ratio 3:6:3:2, respectively. The corresponding ratio determined by simulation of the NMR spectrum was as follows: 3.2:6.3:3.1:1.4, very close to the expected values. Nevertheless, the amount of the Al4 appears somewhat underestimated, presumably due to the fact that the stoichiometry of this site within the structure varies from a sample to sample. Indeed, its relative NMR signal intensity changed significantly for different samples. Since XRD and NMR analyses have been done on two samples from different batches, the stoichiometry of Al4 site could be different.

CO_2 and CH_4 Adsorption Microcalorimetry. The differential enthalpies and isotherms at 30 °C for the adsorption of carbon dioxide and methane are shown in Figure 8, respectively. The adsorption of carbon dioxide occurs essentially below 10 bar with an enthalpy of around 33 kJ·mol^{-1}. The adsorption isotherm of methane is far more linear with an initial interaction of 16 kJ·mol^{-1} which rapidly drops. The amount adsorbed for each gas at 10 bar (4.4 mmol·g^{-1} for CO_2 and 1.95 mmol·g^{-1} for CH_4) is below many materials including zeolites,[72−75] activated carbons,[76−78] and other MOF[35,79] materials.

The initial enthalpies of adsorption of carbon dioxide are very similar to those already observed for previous experiments on MOF samples[35] where initial values were obtained of 35 kJ·mol^{-1} for MIL-53 (Al) and 32 kJ·mol^{-1} for MIL-53 (Cr). These adsorption enthalpies observed are significantly lower than those obtained with aluminosilicate zeolites[72,73] (50−70 kJ·mol^{-1}) and in the same range as those observed for pure silica zeolites such as silicalite.[72] This highlights the relative electronegativity of the MIL-96 framework as the quadrupole moment of the CO_2 molecule would engender stronger interactions, closer to those observed with the aluminosolicate zeolites. The initial enthalpies of adsorption observed for methane on MIL-96 are similar to those previously reported for MIL-53 (17 kJ·mol^{-1}) as well as for the adsorption of methane in the aluminosilicate zeolite NaY[75,78] (17−17.8 kJ·mol^{-1}). These values are all quite similar, emphasizing that the methane molecule, having no permanent moment, is not affected by framework charge. One would expect differences due to strong confinement effects which do not seem to be the case.

Following the return to the baseline of the calorimetric signal gives an indication of the adsorption equilibrium. For the adsorption of carbon dioxide, complete adsorption equilibrium takes ∼1 h for each point. It is noteworthy that for methane adsorption, >5 h were required for the equilibrium of each point. For most porous solids, methane equilibrium is attained after 20 min per point. Such a long time to reach equilibrium is the first time, to our knowledge, that such behavior is observed and should be compared to the hydrogen experiments. Furthermore, the adsorption at room temperature can be compared with nitrogen adsorption at 77 K, and interestingly, almost no uptake

(72) Dunne, J. A.; Mariwala, R.; Rao, M.; Sircar, S.; Gorte, R. J.; Myers, A. L. *Langmuir* **1996**, *12*, 5888.
(73) Dunne, J. A.; Rao, M.; Sircar, S.; Gorte, R. J.; Myers, A. L. *Langmuir* **1996**, *12*, 5896.
(74) Mentasy, L.; Woestyn, A. M.; Basaldella, E.; Kikot, A.; Zgrablich, G. *Ads. Sci. Techn.* **1994**, *11*, 209.
(75) Papp, H.; Hinsen, W.; Do, N. T.; Baerns, M. *Thermochim. Acta* **1984**, *82*, 137.
(76) Buss, E. *Gas Separation & Purification* **1995**, *9*, 189.
(77) Guillot, A.; Follin, S.; Poujardieu, L. *Royal Soc. Chem. − Characterisation of Porous Solids* **1997**, *213*, 573.
(78) Himeno, S.; Komatsu, T.; Fujita, S. *J. Chem. Eng. Data* **2005**, *50*, 369.
(79) Wang, Q. M.; Shen, D.; Bülow, M.; Lau, M. L.; Deng, S.; Fitch, F. R.; Lemcoff, N. O.; Semanscin, J. *Microporous Mesoporous Mater.* **2002**, *55*, 217.

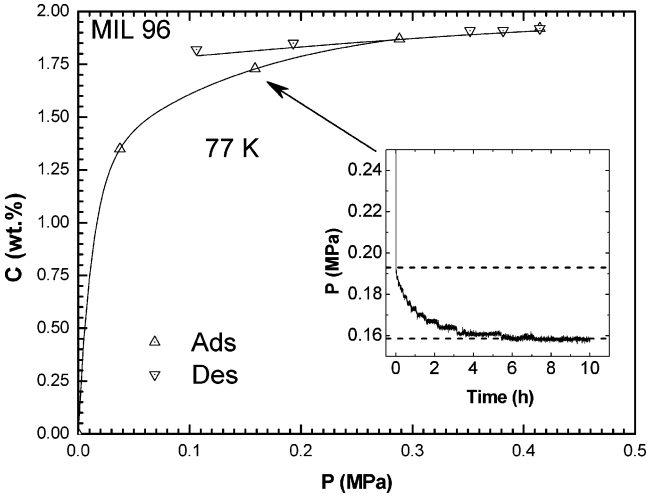

Figure 9. Isotherm curves for the adsorption and desorption of hydrogen on MIL-96 (Al) at liquid nitrogen temperature (the lines are only guides for eyes). (Inset) Hydrogen pressure variation as a function of time for the second adsorption step (see arrow). The final equilibrium pressure (0.159 MPa) corresponds to a capacity of 1.73 wt %. The dashed lines delimit the pressure range between the adsorption processes taking place.

was observed in the latter case, certainly due to the temperature differences of the experiments.

The above-mentioned behavior can be explained by the very small apertures of the pores. Carbon dioxide may be able to enter the apertures due to its smallest dimension of 2.5 Å and due to relatively favorable attraction to the free hydroxyls groups inside the pores. The adsorption of methane is probably hindered by its dimension of 3.8 Å which is very close to that of the pore apertures. It may also be limited by the residual water inside the cages. This presence of water may also explain the limited free volume for both of these probe molecules. Unfortunately, a higher heat treatment leads to a collapse of the structure and no significant adsorption. This is the first of a series of studies with MOF-type materials in which the presence of water either is beneficial or can significantly alter the adsorption of these gases. Nevertheless, it should be noted that saturation is not observed for carbon dioxide and methane adsorption, and a higher adsorption capacity can be expected at higher pressures.

Hydrogen Adsorption. Before the hydrogen adsorption experiments, the MIL-96 (Al) sample was thermally outgassed to remove the water molecules lying within the cages. After a thermal treatment at 150 °C overnight, a weight loss of 18.5% is observed in good agreement with the 19% measured by TGA at 200 °C. The hydrogen uptake was then measured at 77 K. Surprisingly, an unexpected behavior for physisorption was observed with a rather slow adsorption process, and the thermodynamic equilibrium was reached only after 6 to 7 h (Figure 9). This might be due to the small pore opening size of the cavity which would slow the hydrogen diffusion kinetic within the 3D network of the different cages in MIL-96. The adsorption isotherm shows a significant hydrogen uptake at moderate pressure and increases rapidly to reach 1.91 wt %, and a saturation plateau is observed above 0.3 MPa. The desorption branch was tentatively measured down to low pressure, but the reversibility is rather poor, and the sample was not desorbed below 1.82 wt % (Figure 9). Again, the slow desorption kinetic might be attributed to poor hydrogen diffusion kinetics within the framework. The H_2 uptake value is lower than that observed in the porous aluminum terephthalate MIL-53 (3.8% under 1.6 MPa)[34] or some metal−organic framework compounds under higher pressures.[80−82] Nevertheless, it is similar to the storage capacity of other microporous MOF solids such as $Ni(dhtp)(H_2O)_2 \cdot 8H_2O$,[83] Prussian blue analogues,[84] or the NaY zeolite.[85]

Conclusions

Hydrothermal reaction of aluminum nitrate with 1,3,5-benzenetricarboxylic acid (or the methyl ester form, trimethyl 1,3,5-benzenetricarboxylate) in water led to a new aluminum trimesate compound: $Al_{12}O(OH)_{18}(H_2O)_3(Al_2(OH)_4)[btc]_6 \cdot 24H_2O$. The structure, solved by means of single-crystal X-ray diffraction, consists of a 3D framework containing isolated trinuclear μ_3-oxo-bridged aluminum clusters and infinite chains of $AlO_4(OH)_2$ octahedra forming a layerlike hexagonal network based on an 18-membered ring. As far as we are aware, this is the first time that such a μ_3-oxo-centered trinuclear configuration is observed in aluminum chemistry. The organic molecules interact strongly with both the oxo-centered trimeric aluminum units and the 2D network of aluminum octahedra ensuring the cohesion of the structure. Solid-state NMR characterization agrees well with the structure description. The four crystallographic Al sites are resolved in ^{27}Al spectra using 3QMAS. The compound exhibits a hydrogen storage capacity up to 1.91 wt % at 77 K under 3 bar and is able to sorb carbon dioxide (4.4 $mmol \cdot g^{-1}$ at 10 bar) and methane (1.95 $mmol \cdot g^{-1}$ at 10 bar).

The remarkable feature is the occurrence of the μ_3-oxo-centered trinuclear aluminum motif in the structure of MIL-96. Such a trimeric building block was previously described in very promising MOF materials based on super-tetrahedral units for the construction of zeolite-type frameworks with very large pores in MIL-100[9] and MIL-101[10] or solids exhibiting very large swelling effects in the MIL-88 series.[86] Future work will be focused on the isolation of such a triangular unit and its reactivity with the carboxylate ligands. The synthesis of the MIL-100 compound incorporating aluminum is under progress and will be reported soon.[87]

Acknowledgment. T.L. and C.V. thank Dr. Thomas Devic (Versailles) for fruitful discussions. Dr. Claudia Morais is greatly acknowledged for her contribution to this study. T.L., G.F., P.L., and S.B. acknowledge the financial support of the European Community STREP project "DeSANNS" (N*o*. FP6-SES6-020133)).

Supporting Information Available: Crystallographic data in CIF format and figures showing the FAM-II-MQMAS ^{27}Al spectrum, IR spectrum, and TG curve. This material is available free of charge via the Internet at http://pubs.acs.org.

JA0621086

(80) Rowsell, J. L. C.; Yaghi, O. M. *Ang. Chem., Int. Ed.* **2005**, *44*, 4670.
(81) Panella, B.; Hirscher, M.; Pütter, H.; Müller, U. *Adv. Funct. Mater.* **2006**, *16*, 520.
(82) Wong-Foy, A. G.; Matzger, A. J.; Yaghi, O. M. *J. Am. Chem. Soc.* **2006**, *128*, 3494.
(83) Dietzel, P. D. C.; Panella, B.; Hirscher, M.; Blom, R.; Fjellvag, H. *Chem. Commun.* **2006**, 959.
(84) Kaye, S. S.; Long, J. R. *J. Am. Chem. Soc.* **2005**, *127*, 6506.
(85) Langmi, H. W.; Walton, A.; Al-Mamouri, M. M.; Johnson, S. R.; D., B.; Speight, J. D.; Edwards, P. P.; Gameson, I.; Anderson, P. A.; Harris, I. R. *J. Alloys Compd* **2003**, *356−357*, 710.
(86) Mellot-Draznieks, C.; Serre, C.; Surblé, S.; Audebrand, N.; Férey, G. *J. Am. Chem. Soc.* **2005**, *127*, 16273.
(87) Volkringer, C.; Loiseau, T.; Haouas, M.; Taulelle, F.; Férey, G. *in preparation* **2006**.